Journal of Materials Chemistry B

RSC Publishing

PAPER

Aggregation induced photodynamic therapy enhancement based on linear and nonlinear excited FRET of fluorescent organic nanoparticles†

Cite this: *J. Mater. Chem. B*, 2013, **1**, 2350

Meng-Chieh Hsieh,[a] Cheng-Hao Chien,[bc] Cheng-Chung Chang*[a] and Ta-Chau Chang[bc]

Received 1st November 2012
Accepted 5th March 2013

DOI: 10.1039/c3tb00345k

www.rsc.org/MaterialsB

A binary molecule can self-assemble to form fluorescent organic nanoparticles (FONs) based on the Aggregation-Induced Emission Enhancement (AIEE) property and subsequently, presents an efficient fluorescence resonance energy transfer (FRET) to generate singlet oxygen under linear and nonlinear light sources. Biologically, this FON-photosensitizer is much more phototoxic to cancer cells than to normal cells without significant dark toxicity. Eventually, a new approach, called FON FRET-PDT or AIEE FRET-PDT, to promote the PDT effect is expected.

Introduction

Fluorescent organic nanoparticles (FONs), which have recently received a considerable amount of attention, are expected to function in a wide variety of applications because the synthetic approaches are flexible for these organic compounds.[1,2] Notably, studies on the application of FONs in cancer cell detection and diagnosis are lacking. In previous studies, we developed FON models for anionic and cationic organic dyes by using their aggregation-induced emission enhancement (AIEE) properties, and described their application in cellular staining.[3] We then developed a vacuole model using FONs to elucidate the formation of fluorescent bright spots that are thought to form in the lysosomes of cancer cells and have been identified for specific cancer cell recognition.[4] In this study, we attempted to establish a concept that takes advantage of FONs in photodynamic therapy (PDT) drug potency because in most cases, the aggregation of the photosensitizer usually decreases the quantum yields of fluorescence and singlet oxygen generation,[5] especially in nanocarrier incorporated-photosensitizer systems. This phenomenon will result in an incomplete release or significant reduction of the photodynamic activity by self-photoquenching.[6] Therefore, once the molecular aggregation behavior was found, whatever has been characterized in aqueous or nonaqueous medium should be considered in the cell and its phototoxicity should also be evaluated.[7]

Recently, the disadvantage of PDT caused by aggregation of the photosensitizer has been diminished by the FRET-PDT binary system model by the use of quantum dots[8] or two-photon absorbing chromophores[9] as a FRET donor to indirectly activate the acceptor photosensitizer. These binary systems can not only decrease the aggregation tendency of photosensitizers but are also able to support a new optical window for cancer imaging and therapies.[10] Here, combining the FRET-PDT and FON models, we expect that the emission of the FRET donor increases due to its AIEE property while the aggregation of the FRET acceptor (photosensitizer) decreases.

That is, once the FRET-PDT system forms a fluorescent nanoparticle based on AIEE behavior, a new approach (called FON FRET-PDT or AIEE FRET-PDT) to promote the PDT effect is expected. In this manuscript, a binary conjugate was constructed with a FRET donor (BMVC, 3,6-bis-(1-methyl-4-vinylpyridinium)-carbazole diiodide) and an FRET acceptor (porphyrin or metalloporphyrin), as shown in Scheme 1. The former acts as a linear and nonlinear light capturing antenna, factor of AIEE, FRET donor and supports the specific recognition of these binary conjugates for cancer cells; the latter acts as a FRET acceptor and the photoactive center of the binary complex to generate singlet oxygen. The strategy is: the binary conjugate can self-assemble to form FONs which result from the AIEE of the BMVC moiety but not the porphyrin moiety. The AIEE from the aggregated BMVC induced efficient FRET to the non-aggregated porphyrin, and then to efficiently generate singlet oxygen. Furthermore, the FRET efficiency is a critical factor that depends on the overlap between the emission energy of BMVC and the excitation cross-section of porphyrin. To fit the BMVC emission and improve the FRET efficiency of the binary molecule, we consider metalloporphyrin as the acceptor and evaluate the PDT efficiency.

[a]*Graduate Institute of Biomedical Engineering, National Chung Hsing University, 250 Kuo Kuang Road, Taichung, 402, Taiwan, ROC. E-mail: ccchang555@dragon.nchu.edu.tw; Fax: +886-4-22852422*

[b]*Institute of Atomic and Molecular Sciences, Academia Sinica, P.O. Box 23-166, Taipei 106, Taiwan, ROC*

[c]*Institute of Biophotonics, National Yang-Ming University, Taipei 112, Taiwan, ROC*

† Electronic supplementary information (ESI) available: Fig. S1–S4, Videos S1–S3 and their caption. See DOI: 10.1039/c3tb00345k

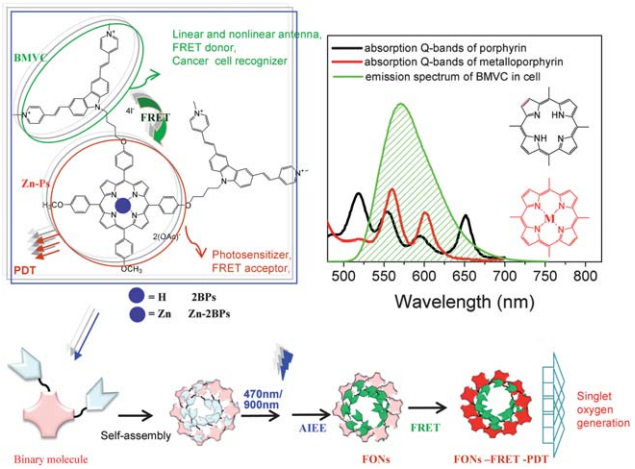

Scheme 1 The structure of binary compound **Zn-2BPs** (Ps: porphyrin) and the FRET schematic diagram between the emission spectrum and porphyrin or metalloporphyrin.

Molecule design

A previous study has shown that substituting two BMVC molecules at the 5- and 10-positions of tetra-phenyl porphyrin (product named **2BPs**, Scheme 1) presented the optimal PDT effect based on the biological evaluation from their structure–activity relationship.[11] As we mentioned above, to improve the FRET ratio of the **2BPs**, we consider metalloporphyrin as the acceptor. It is known that the presence and nature of the central metal ion, which is bound by a number of photosensitizers, strongly influence the photophysical properties of the photosensitizer.[12] To date however, for porphyrin derivatives, there has been no consistent observation as to the potential success of metallated photosensitizers. Therefore, before synthesizing the binary system, we prepared various tetraphenyl-metalloporphyrins and determined the most suitable acceptor based on the criteria of the absorption energy of the Q-bands and singlet oxygen yields (Fig. 1). Furthermore, for physiological consideration, zinc is more suitable than cadmium. This is why **Zn-2BPs** was prepared and eventually, more efficient FRET is expected because of either the linear or nonlinear optical properties.

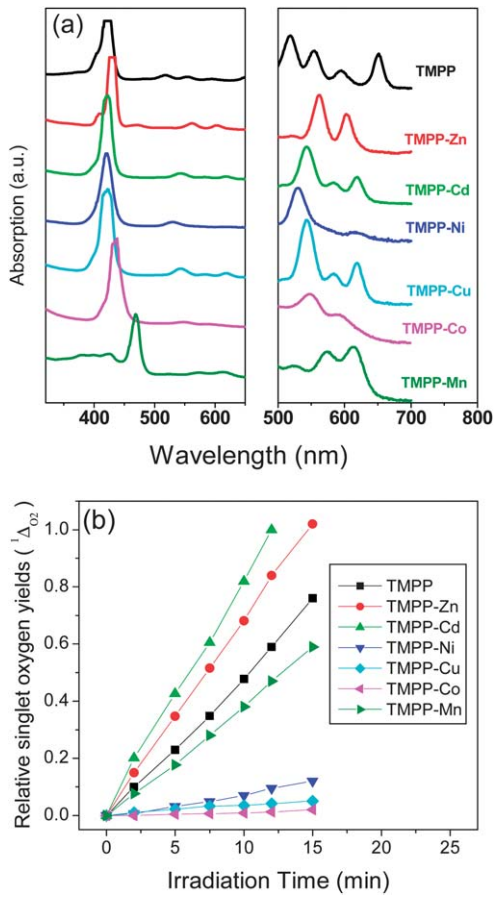

Fig. 1 (a) The UV-vis absorption spectra and (b) relative singlet oxygen yields ($^1\Delta_{O_2}$) of metalloporphyrin derivatives under white light (400–700 nm). TMPP: metallotetraphenyl-porphyrins.

Experimental section

1 Materials

The general chemicals employed in this study were of the highest grade available and were obtained from Acros Organic Co., Merck Ltd, or Aldrich Chemical Co. and used without further purification. All of the solvents were of spectrometric grade.

2 Apparatus

The absorption spectra were generated using a Thermo Genesys 6 UV-visible spectrophotometer, and the fluorescence spectra were recorded using a HORIBA JOBIN-YVON Fluoromas-4 spectrofluorometer with a 1 nm band-pass and a 1 cm cell length at room temperature. Transmission electron microscopy (TEM) was performed on a Zeiss EM 902A operated at 80 kV. A mixed solution (a mixed solvent of THF and deionized water, 50/50, v/v) that contained the compound was deposited onto a carbon-coated copper grid. Nanoparticle sizes and sizing partition curves were directly measured using NanoSight LM20 and NTA 2.0 Analytical Software in the same solution. The cellular fluorescence images and dual staining fluorescence images were taken using a Leica AF6000 fluorescence microscope with a DFC310 FX Digital color camera and the λ scanning was taken using the Leica TCS SP5 confocal fluorescence microscope. The excitation source was a 488 nm Ar laser for the compounds. Fluorescence photographs were taken through the related wavelength ranges using photomultiplier tubes (PMT). The light source used to measure the singlet oxygen yield and PDT cell death was the Xenon Light Source LAX-Cute (Asahi Spectra). For two-photon excitation, we used a Ti-sapphire laser (Mira-900F, Coherent, USA) at 900 nm wavelength, which was directed into a laser scanning microscope (FV300 and IX-71, Olympus, Japan) and focused onto the sample using a 60× (N.A. = 1.2) water immersion objective (UPLSAPO 60XW, Olympus, Japan).

3 Cell culture conditions and compound incubation

The human embryonal lung MRC-5 normal fibroblast cells and HeLa human cervical cancer cells were maintained in Modified Eagle's Medium (MEM) containing non-essential amino acids,

Earle's salts, L-glutamine, 1 mM sodium bicarbonate, 1 mM sodium pyruvate, 1% (penicillin + streptomycin) and 10% fetal bovine serum (FBS); the human lung adenocarcinoma cell line CL1-0 was maintained in RPMI-1640 medium containing 1% (penicillin + streptomycin), sodium bicarbonate (2.0 g L^{-1}) and 10% FBS. The cells were cultured at 37 °C in a humid atmosphere with 95% air and 5% CO_2. Before the observation of cellular localization, the cells were seeded onto coverslips and incubated for 24 h. The next day, cells were incubated with different concentrations of compounds for 12 h, for which the DMSO stock solutions were diluted in serum-free medium before use (1/100 v/v).

4 Measurement

The light source for measurement of the singlet oxygen yield and PDT cell death was a white light (a 20 W xenon lamp that passes through a 400–700 nm mirror module). Before the light was output from the optional light guide and collimator lens, the light passed through a 470 nm band pass (bp) filter (the light power was 30 μW cm^{-2} on the dish surface). The singlet oxygen quantum yields from compounds that were in an organic solvent or a mixed solution (THF/deionized water, FON conditions) were determined by a photo-steady-state method using 1,3-diphenylisobenzofuran as the scavenger. The critical micelle concentration was measured by monitoring the ratios of emission intensities after excitation at 470 nm and Soret band (I_{470}/I_{soret}) and observing the breakpoints in the fitting curves. Dual staining of the tracker and compound: the cells were first incubated with the compound for 12 hours, which was followed by incubation with 5 μM organelle probes (MitoTracker green FM for 20 min at 37 °C, LysoTracker green DND-99 for 30 min at 37 °C), and then washed with PBS before observation. The excitation source was a green light cube, in which the light passed through a 530/20 nm bp filter and the emission was collected through a 590 nm lp filter (red emission of compound) and a blue light cube, in which light passed through a 480/10 nm bp filter and the emission was collected through a 510 nm lp filter to collect green emission of probes. Once the definite yellow color image was obtained, we said that the compound was co-localized with the probes. PDT-induced phototoxicity was determined using propidium iodide under a fluorescence microscope (excitation/emission maxima ~535/617 nm) and confirmed by Trypan blue exclusion and staining assay. For two-photon excitation-PDT experiment, the cells were plated on a μ-slide (80826, ibidi GmbH, Germany) and were incubated with or without 5 μM of **Zn-2BPs** for five hours. Prior to the experiment, the cells were washed twice with phosphate buffered saline (PBS), and then refilled with fresh medium with 0.01 mg mL^{-1} propidium iodide (PI, P3566, Invitrogen, USA), which was used to detect dead cells. The laser exposure time was 2 ms per pixel. The fluorescence from **Zn-2BPs** and propidium iodide was detected by the same objective through epi-detection, passing through a 685 nm short-pass dichroic mirror (685SPXR, Chroma, USA) and a 694 nm short-pass filter (FF01-694/SP, Semrock, USA), detected using a PMT (R3896, Hamamatsu, Japan). In the image/video the fluorescence was pseudo-colored in yellow.

5 Synthesis of the binary conjugates

Scheme 2 shows the synthesis of two binary conjugates. The detailed synthesis procedures for 2-BPs and compound **3** have been described previously [ref. 11]. The compound zinc(II) *o*-5,10-bis(4-(3,6-bis-(-2-(1-methylpyridium-4-yl)vinyl)-9*H*-carbazol-9-yl-butoxyl)phenyl)-15,20-bis(4-methoxylphenyl)porphyrin iodine (**Zn-2BPs**) is prepared as follows. A solution of compound **3** (0.2 mmol) in 70 mL of dichloromethane was treated with 30 mL of a saturated solution of zinc(II) acetate in methanol. The mixture was stirred overnight at room temperature. After that, the solution was treated with water (200 mL) and the organic phase was extracted with three portions of dichloromethane (50 mL each). The solvents were evaporated under reduced pressure and compound **4** was collected with a high yield from compound **3**. Data for compound **4**: ^{1}H-NMR (400 Hz, DMSO, δ): δ (ppm) = 8.764 (d, J = 4.4 Hz, 4H), 8.744 (d, J = 4.4 Hz, 4H), 8.544 (d, J = 2 Hz, 4H), 8.474 (d, J = 4 Hz, 8H; pyridine H), 8.052 (d, J = 8 Hz, 4H; Ar H), 8.007 (d, J = 8 Hz, 4H; Ar H), 7.869 (dd, J = 2 Hz, J = 8 Hz, 4H), 7.802 (d, J = 8.8 Hz, 4H), 7.756 (d, J = 16.4 Hz, 4H; vinyl H), 7.542 (d, J = 4.8 Hz, 8H; pyridine H), 7.326 (d, J = 8 Hz, 4H; Ar H), 7.280 (d, J = 16.8 Hz, 4H; vinyl H), 7.249 (d, J = 8.8 Hz, 4H; Ar H), 4.608 (t, J = 6.8 Hz, J = 6.8 Hz, 4H), 4.227 (t, J = 6.8 Hz, J = 6.8 Hz, 4H), 4.014 (s, 6H; OCH_3H), 2.104 (m, 4H), 1.914 (m, 4H). HRMS (ESI, m/z): $[M + H]^+$ 1625.24; found, 1623.0; anal. calcd% for $C_{106}H_{82}N_{10}O_4Zn$: C, 78.34; H, 5.09; N, 8.62. **4**·(H_2O + CH_3COOH): $C_{108}H_{88}N_{10}O_7$: C, 76.16; H, 5.21; N, 8.22. Found, C, 76.03; H, 5.28; N, 8.20%. After refluxing compound **4** with excess CH_3I in THF, the final products of **Zn-2BPs** were collected as orange-purple powders that were recrystallized twice from acetone. Data for **Zn-2BPs**: ^{1}H-NMR (400 Hz, DMSO, δ): δ (ppm) = 8.819 (d, J = 4 Hz, 4H), 8.794 (d, J = 4 Hz, 4H), 8.781 (d, J = 4.4 Hz, 8H; pyridine H), 8.682 (d, J = 2 Hz, 4H), 8.261 (d, J = 16 Hz, 4H), 8.221 (d, J = 5.2 Hz, 8H; pyridine H), 8.063 (d, J = 8 Hz, 4H), 8.043 (d, J = 8 Hz, 4H), 8.033 (d, J = 8.8 Hz, 4H; Ar H), 7.967 (d, J = 8.8 Hz, 4H; Ar H), 7.596 (d, J = 16 Hz, 4H; vinyl H), 7.346 (d, J = 8.4 Hz, 4H; Ar H), 7.315 (d, J = 8.4 Hz, 4H; Ar H), 4.707 (t, J = 6.4 Hz, J = 6.4 Hz, 4H), 4.295 (t, J = 6.4 Hz, J = 6.4 Hz, 4H), 4.228 (s, 12H, CH_3I), 4.032 (s, 6H; OCH_3 H), 2.160 (m, 4H), 1.973 (m, 4H). HRMS (ESI, m/z): $[M + H]^+$ 1670.34 (exclude I^-); found, 1665.27; anal. calcd % for $C_{110}H_{94}I_4N_{10}O_4Zn$: C, 60.25; H, 4.32; N, 6.39. **Zn-2BPs·3H$_2$O**: $C_{110}H_{110}I_4N_{10}O_4Zn$: C, 58.80; H, 4.49; N, 6.23. Found, C, 58.19; H, 4.51; N, 6.18%.

Results and discussion

1 Basic photophysical properties and FRET investigation

Fig. 2(a) presents the absorption (435 nm, Soret band; 564, 605 nm Q-band) and emission (613, 665 nm) spectra of the **Zn-2BPs** product in a DMSO solution. Compared to 2-BPs, compound **Zn-2BPs** showed a red-shift in the absorption Soret band, while a blue-shift in emission with lower intensity. No emission signal from BMVC was observed under these conditions. However, the evidence of FRET was supported from the experimental results shown in Fig. 2(b). Both the plots of excited wavelength-dependent emission intensities at 613 nm (a plot of emission

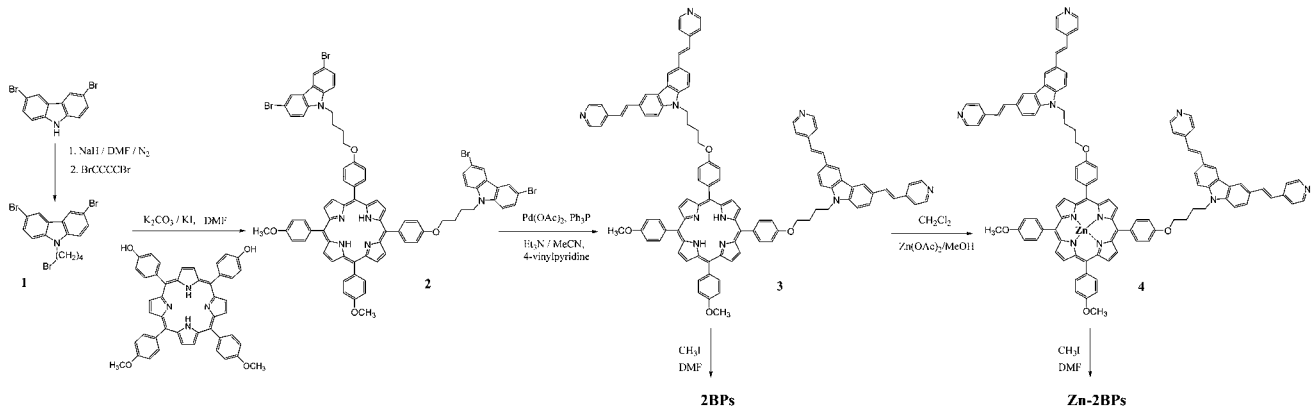

Scheme 2 Synthesis procedure for the binary conjugates: **2BPs** and **Zn-2BPs**.

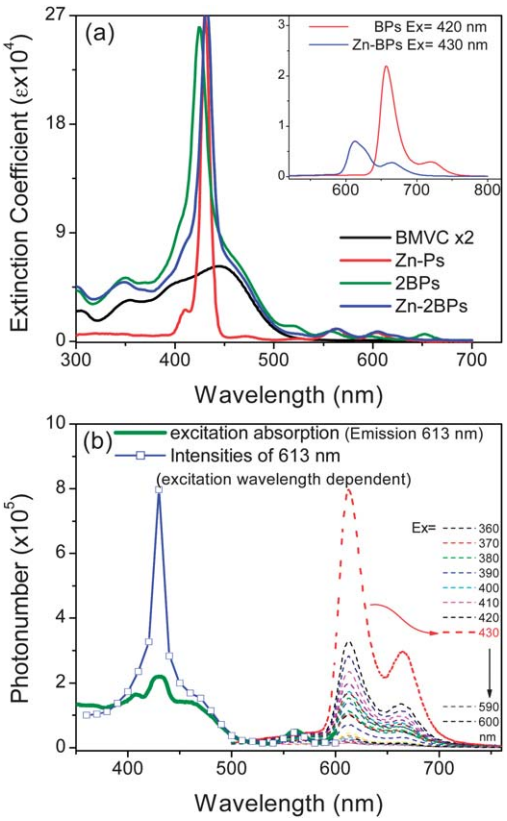

Fig. 2 (a) The extinction representation of the absorption spectra of BMVC, Zn-Ps, **2BPs** and **Zn-2BPs**. The inset shows the emission curves of **2BPs** and **Zn-2BPs**. (b) The fluorescence excitation spectrum of 1 μM **Zn-2BPs** (green line) and the plot of excited wavelength-dependent emission intensities at 613 nm from excitation at 360 to 600 nm.

maximum values against excited wavelength every 10 nm ranging from 360 to 600 nm, blue line) as well as the fluorescence excitation spectrum (green line, recording the emission intensity at 613 nm wavelength) of **Zn-2BPs** are similar to their absorption spectrum pattern shown in Fig. 2(a). The experimental results suggest that the emission of the metalloporphyrin part in **Zn-2BPs** can be induced by excitation at 450–500 nm, which corresponds to the absorption region of BMVC and the window of transparency for porphyrin and metalloporphyrin derivatives.

2 Investigation of the aggregation-induced emission enhancement (AIEE) and evolution of the fluorescent organic nanoparticles (FONs)

The AIEE phenomena were conveniently demonstrated by examining the emission spectra of the compound in various ratios of H_2O–THF (tetrahydrofuran) solvents.[1,2] Fig. 3(a) reveals that the fluorescence intensities of **Zn-2BPs** reached their maximum values in an aqueous solution with a 50% THF volume fraction, with more apparent emission peaks in the 500–600 nm range than in Fig. 2, and the corresponding TEM image clearly revealed fine spherical-shaped nanoparticles. Fig. S1† indicates that the mean diameter of the corresponding FONs can range from ~50 nm (lower preparation concentration, 1 μM) to ~560 nm (higher preparation concentration, 100 μM). Although the sizes of the nanoparticles were dependent on the concentration of the preparation solution, the fluorescence emitting wavelengths were almost constant (Fig. 3(b)). Furthermore, the inset of Fig. 3(b) showed that the larger size FONs can be easily prepared and observed using fluorescence microscopy. Based on the previous studies, we inferred that the **Zn-2BPs** compounds could serve as surfactant-like molecules that can further self-assemble to form micelle-like nanoparticles due to their amphiphilic nature[11] (hydrophilic BMVC and hydrophobic porphyrin, results for determining the critical micelle concentration and a detailed experimental protocol are shown in Fig. S2†). Furthermore, it is likely that the FONs formed from either packing or crowding of the BMVC moiety, whose rotation along the molecule axis was constrained, and then the thermal relaxation of the excited state was decreased.[13] Fig. S3† clearly shows that, based on the similar AIEE examining protocol, BMVC offered a tendency towards FONs, but porphyrin didn't. Hence, we proposed that the fluorescence intensity of BMVC will enhance when molecules aggregate while the fluorescence intensity of porphyrin will self-quench when molecules aggregate with increasing concentration. That is why, in Fig. 3(b), the compound **Zn-2BPs** showed a concentration-dependent nonlinear fluorescence enhancement. Consequently, a low emission BMVC monomer became a green

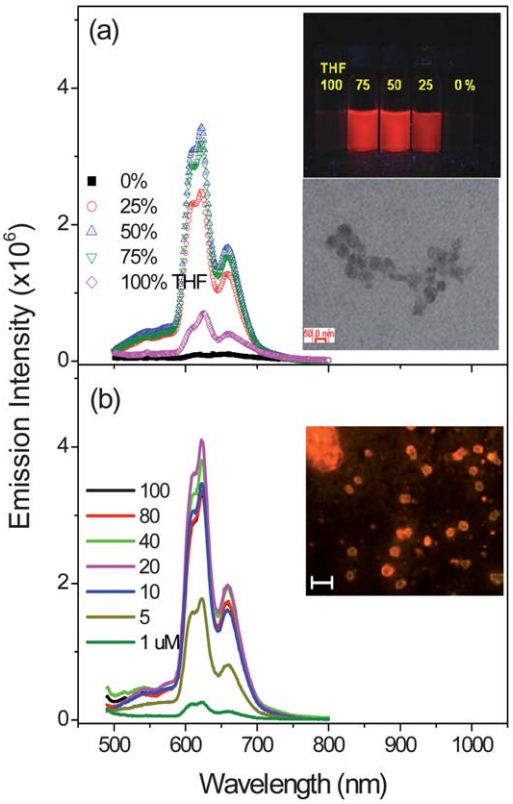

Fig. 3 (a) FON illustrations for 10 μM of the compound **Zn-2BPs**. Emission spectra variations with aqueous solutions that contained 0, 25, 50, 75 and 100 percentages of THF (Ex = 470 nm). The relative visible emission photographs under UV light (365 nm) and TEM images (scale bar: 50 nm). (b) Concentration effect spectra of FONs (50 percentages of THF aqueous solutions, Ex = 470 nm) and the fluorescent microscopy images which were obtained from 100 μM FON solution (excitation: 480/10 nm bp filter, emission: 510 nm lp filter, and scale bar: 1 μm).

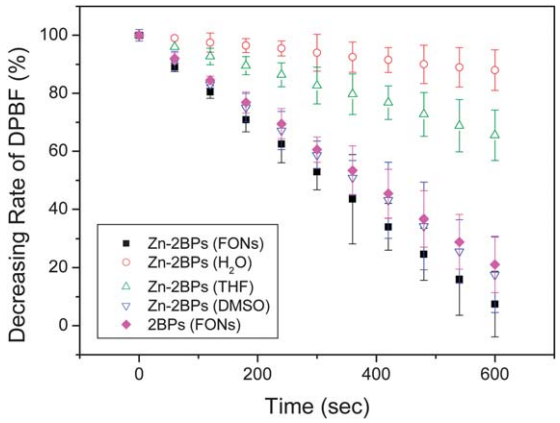

Fig. 4 Relative DPBF oxidation rates by singlet oxygen that was generated from the photosensitizers after irradiation with a 20 W xenon lamp. The final output light power was 50 μW cm^2 for the 470 nm bp filter through the fiber. 15 μM of the respective dyes were mixed with 500 μM of DPBF in the mixed solution (THF/H_2O = 50/50, v/v), and the absorbance readings for DPBF (390 nm) were recorded from 1 to 10 min. Each data point represents the average from three separate experiments.

emitting fluorophore under the AIEE conditions. That is why we call BMVC the AIEE factor of the binary conjugate. The AIEE phenomenon of the BMVC moiety resulted from the aggregation of **Zn-2BPs**, and its fluorescence enhancement was dependent on the size of the particles but the emission wavelengths were independent of the particles.

3 Singlet oxygen generation and intracellular accumulation

Fig. 4 presents the DPBF oxidation rates of **Zn-2BPs** under the FON conditions when excited at 470 nm (THF/H_2O = 1/1, v/v). It is clear that the FONs formed of Zn-BPs exhibited a greater singlet oxygen yield than this compound under the H_2O and THF conditions. In fact, the quenching of DPBF by singlet oxygen is inhibited by H_2O. Hence, based on our result, we believe that the singlet oxygen yield of the compound in THF–H_2O mixing solution is better than in DMSO. On the other hand, considering the deviation error bars of these data, we do not judge that the singlet oxygen yield of **Zn-2BPs** is better than **2BPs** under FONconditions. Though we conclude temporarily that Zn-BPs is better than **2BPs** due to a higher FRET efficiency, nevertheless, in Fig. 4, we want to show that the singlet oxygen yield of the compound in FONs formed is better than the monomer.

As described above, **Zn-2BPs** is a binary compound containing molecules of BMVC (green light) and metalloporphyrin (red light); and the fluorescent intensities of BMVC vary with aggregation degrees. Hence, the evaluation of cellular uptake requires additional investigation. At first, the apparent fluorescent signals at 500–600 nm, when we collected λ scanning spectra of **Zn-2BPs** in HeLa cancer cells using confocal microscopy, revealed that there were at least two sets of emission enhancements (Fig. 5(a)), which both presented more apparent BMVC emission intensities than the spectra shown in Fig. 3. We inferred that the unusual emission enhancement may due to the different degrees of FON formation of **Zn-2BPs**, which resulted in the AIEE phenomena and occurred more frequently than we expected in the HeLa cancer cells and was observed in the spectra. Hence, when we examined the cellular uptake of **Zn-2BPs**, we measured the fluorescent signals using a red filter (590 nm long pass to detect the emission for porphyrin) and a green filter (510 nm long pass to detect the emission for BMVC + porphyrin). It is clear that more of this compound accumulated in the CL1-0 lung cancer cells than in the MRC-5 normal lung cells in both cases (Fig. 5(b)). Based on the description of Fig. 5(a), the difference in the uptake between these two cancer cells and the MRC-5 cells was more apparent when the signals were collected with the green filter.

4 Linear and nonlinear phototoxicity

Fig. 6 reveals that no significant dark phototoxicity was observed for the MRC-5 normal cells after treatment with **Zn-2BPs**, whereas distinct PDT effects were observed for the HeLa cancer cells after being irradiated with a 470 nm band pass light source. This figure also reveals that the FRET-PDT of **Zn-2BPs** was better than that of **2BPs** with unapparent dark toxicity. A similar phototoxicity result was observed when the system was irradiated under white light (400–700 nm) as the PDT light

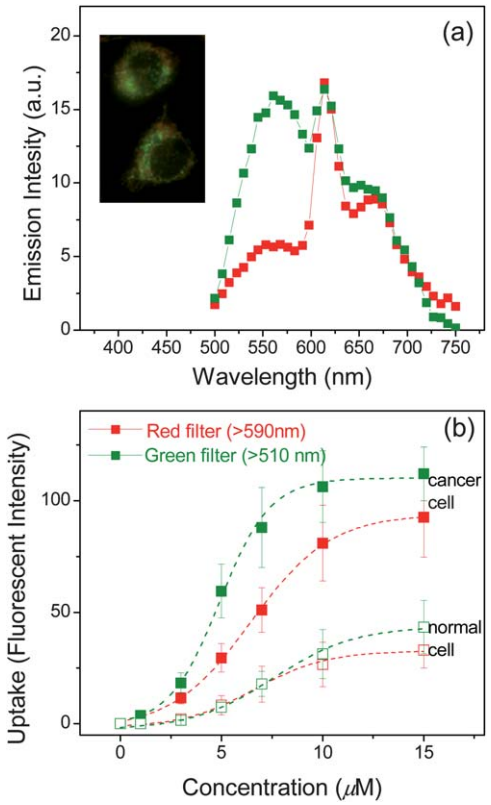

Fig. 5 (a) Two sets of spectra representations from λ scanning of confocal microscopy images of the HeLa cancer cells. The spectra were obtained from the average of 30 individual cancer cells. (b) Intracellular accumulation of **Zn-2BPs** in MRC-5 normal and CL1-0 cancer cells. The cells were incubated with various concentrations of the compound for 12 h, and the intracellular uptake was determined from a fluorescence calibration curve. Each data point represents the average from three separate experiments and dashed lines indicate fitting curves.

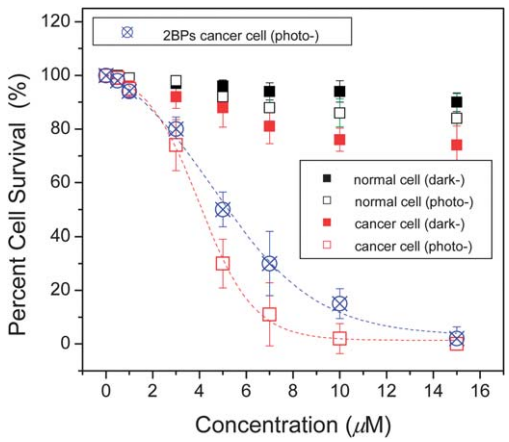

Fig. 6 Phototoxicity of HeLa cancer cells treated with **Zn-2BPs** (0.5, 1, 3, 5, 7, 10 and 15 μM, incubated for 12 h before irradiation) and irradiated with a 470 nm band pass light source (30 μW cm^{-2}) for 5 min; cell death was tested overnight. Each data point represents the average from three separate experiments and dashed lines indicate fitting curves.

source. Fig. 7(a) illustrates the FRET-PDT color switch process from a real-time video recorded under a fluorescence microscope with a color CCD (Videos S1and S2†); it is clear that the cells form blebs during the late stage of irradiation and can be easily stained with propidium iodide (Fig. S4†). Thus, we inferred that the significantly faster photoinduced translocation was because the nuclear membrane was damaged during the irradiation period and then the compound was translocated into the nucleus, which results in a strong green emission in the nucleus. Based on the previous studies, it is known that the fluorescence of BMVC increases by two orders of magnitude upon interaction with DNA in the nucleus.[14] The excellent contrast during the cellular imaging of this compound can serve as a cell death biomarker for the study of PDT.

Furthermore, BMVC has a large cross-section for two-photon absorption at approximately 860–920 nm,[15] which is a wavelength range that is close to the optimal wavelength required for penetrating the tissue to excite the photosensitizer. Thus, during a nonlinear PDT test, the real-time video in Fig. 7(b), which was collected using a 900 nm picosecond Ti-sapphire laser beam as the light source, presented a similar result as Fig. 7(a) and similar photo-toxicity as Fig. 6. These real time two-photon images clearly showed that the signals of BMVC disappeared in the cytoplasm but appeared in the nucleus with irradiation. That is, we provided an additional PDT light window in the 450–500 nm and 800–900 nm ranges, which is absent in porphyrin and generates efficient PDT without appreciable side effects in MRC-5 normal cells. Here, we must claim that (1) we want to emphasize that photo-induced cell death accompanied by color-change or photo-induced translocation phenomena, color CCD with a long-pass filter is necessary. (2) This phenomenon of this compound happens too fast under the laser sources (405 or 488 nm laser), and it is hard to collect the video results in Fig. 7(a) under a confocal system (that is why we presented videos). (3) In the two-photon system, photo-induced color change became slower and we can collect the video between the PDT periods with a self-fabricated Ti-sapphire laser collocating a mono-color CCD (pseudo-color in Fig. 7(b)). (4) The double-staining protocol is unsuitable in performing Fig. 7, because the staining of nuclear probes (Hoechst or PI) will interrupt the color presentation, that is why we present the bright-field image.

5 Sub-cellular localization

We have explained that why fluorescence microscopy measurement is more suitable than confocal measurement in our case. For a binary compound which contains a green emission BMVC and a red emission metalloporphyrin, its intracellular fluorescent signals vary during irradiation. The sub-cellular localization of this compound is difficult to carry out. Furthermore, the green and red filters captured the fluorescence from the tracker green and metalloporphyrin portion of **Zn-2BPs**, respectively. Primarily, the red filter exposure time was approximately 3–4 times longer than the green filter and then it was possible to enhance the FRET image signal for the metalloporphyrin whose emission overlapped with the tracker red fluorescence. That is why dual staining was not successful for these conjugates using MitoTracker Red or LysoTracker Red. Hence, to determine the localization of each compound, as

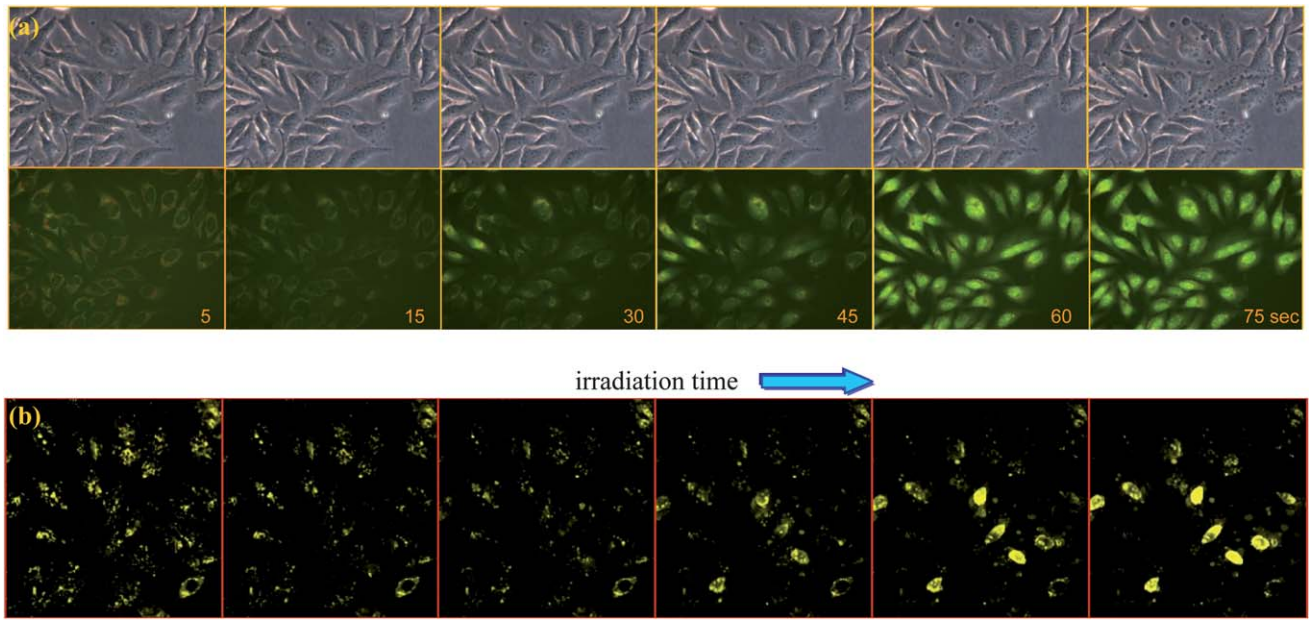

Fig. 7 (a) Several selected fluorescent and bright-field images from a real-time video (Videos S1 and S2†) for photo-induced translocations of a 10 μM compound (fluorescence images were excited by a blue light cube that passed light through a 480/10 nm bp filter, and the emission was collected through a 510 nm lp filter of a fluorescent microscope). (b) Experiment similar to that presented in (a) but with the use of a Ti-sapphire laser at a wavelength of 900 nm as the light source (Video S3†). In the image/video the fluorescence was pseudo-colored in yellow from a mono-color CCD.

detailed in the Experimental section, the cell incubated with compound **Zn-2BPs** was double stained with the cellular tracker green, which merged with the red light emission region of **Zn-2BPs**. Fig. 8 reveals that **Zn-2BPs** may be localized predominantly in mitochondria and lysosome. Generally, mitochondrial photodamage has been reported to be the primary cause of apoptosis during PDT because mitochondria play an integral role in various cell biological processes, such as energy production, apoptotic cell death, molecular metabolism, calcium signaling, and cell redox status.[16,17] However, lysosomal photodamage has also been reported to induce apoptosis in PDT, although this sub-cellular localization has been attributed to either the relocalization of the photosensitizers to mitochondria or the destabilization of the photosensitizers after the PDT process.[16,18] Consequently, mitochondria and lysosomes are very attractive sites for the localization of the photosensitizers to improve the efficiency of the PDT. Indeed, we have double-stained this compound with other probes and only mitotracker and lysotracker found the possible co-localization merge images.

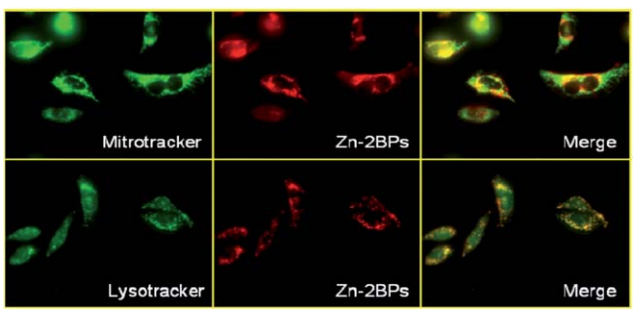

Fig. 8 Sub-cellular localization of Zn-BPs in HeLa cancer cells from fluorescent microscopy. The images of the green tracker were excited by a blue light cube that passed light through a 480/10 nm bp filter, and the emission was collected through a 510 nm lp filter. The red images of the compound were excited by a green light cube that passed light through a 530/20 nm bp filter, and the emission was collected through a 590 nm lp filter.

It is interesting that the PDT effects of **2BPs** and **Zn-2BPs** are better than what we expected. Hence, we try to analyze the phototoxicity efficiency and possible mechanism of **Zn-2BPs**. In a previous study we investigated that the extra phototoxic effect of **2BPs** could result from a photo-induced reaction of BMVC in addition to its dark toxicity.[11] Recently, we found that light-induced photo-reduction of BMVC generated an apparent increase in the signal from the free radical probe 4-((9-acridinecarbonyl) amino)-2,2,6,6-tetramethylpiperidin-1-oxyl (TEMPO-9-ac, Invitrogen, Carlsbad, CA), as the most PDT type I cases.[19] Meanwhile, PDT protocols showed that BMVC-PDT treatment significantly inhibited the growth of tumor cells both in the *in vitro* and *in vivo* studies. Eventually, we have successfully applied BMVC for tumor targeting markers and treatment and demonstrated that BMVC may be a potent tumor-specific photosensitizer for PDT.[20] That is why the PDT efficiency of the BMVC–porphyrin binary conjugate is much better than porphyrin and additionally, **Zn-2BPs** is better than **2BPs** with more effective FRET effect.

Conclusion

In summary, the **Zn-2BPs** compound was designed to offer better FRET efficiency between BMVC and metalloporphyrin. The key function is that the **Zn-2BPs** can self-assemble to form FONs that result in AIEE *in vitro* and in the cells. Consequently, the FRET occurred from the aggregated BMVC to the

metalloporphyrin and generated additional singlet oxygen for efficient PDT. Therefore, the PDT characteristics of the **Zn-2BPs** compound include (1) both target and irradiation wavelength selectivity for the PDT of HeLa and CL1-0 cancer cells; (2) excellent contrast during cellular imaging, which can be applied to monitor the pathway of PDT and serve as a cell death marker; (3) similar PDT behavior under linear and nonlinear (two photon emission) light sources; (4) diminished the aggregation-induced PDT disadvantage; and (5) BMVC supported extra phototoxicity.

This work was supported financially by the National Science Council (NSC-100-2218-E001-001) and (NSC 101-2113-M-005-016-MY3) of Taiwan.

Notes and references

1 (*a*) H. S. Nalwa, H. Kasai, S. Okada, H. Oikawa, H. Matsuda, A. Kakuta, A. Mukoh and H. Nakanishi, *Adv. Mater.*, 1993, **5**, 758–760; (*b*) H. B. Fu and J. N. Yao, *J. Am. Chem. Soc.*, 2001, **123**, 1434–1439.

2 (*a*) B. K. An, S. K. Kwon and S. Y. Park, *Angew. Chem., Int. Ed.*, 2007, **46**, 1978–1982; (*b*) J. Luo, Z. Xie, J. W. Y. Lam, L. Cheng, H. Chen and C. Qiu, *Chem. Commun.*, 2001, 1740–1741; (*c*) D. Xiao, L. Xi, W. Yang, H. Fu, Z. Shuai, Y. Fang and J. Yao, *J. Am. Chem. Soc.*, 2003, **125**, 6740–6745; (*d*) S. S. Palayangoda, X. Cai, R. M. Adhikari and D. C. Neckers, *Org. Lett.*, 2008, **10**, 281–284.

3 (*a*) S. Y. Su, H. H. Lin and C. C. Chang, *J. Mater. Chem.*, 2010, **20**, 8653–8658; (*b*) H. H. Lin, Y. C. Chan, J. W. Chen and C. C. Chang, *J. Mater. Chem.*, 2011, **21**, 3170–3177.

4 H. H. Lin, S. Y. Su and C. C. Chang, *Org. Biomol. Chem.*, 2009, **7**, 2036–2039.

5 J. Moan, K. Berg and V. Iani, Action spectra of dyes relevant for photodynamictherapy, in *Photodynamic tumour therapy 2nd and 3rd generation photosensitizers*, ed. J. G. Moser, Harwood Academic Publishers, Amsterdam, 1998, pp. 169–181.

6 S. Hackbarth, V. Horneffer, A. Wiehe, F. Hillenkamp and B. Roder, *Chem. Phys.*, 2001, **269**, 339–346.

7 B. C. Bae and K. Na, *Biomaterials*, 2010, **31**, 6325–6335.

8 (*a*) S. Moeno, E. Antunes, S. Khene, C. Litwinski and T. Nyokong, *Dalton Trans.*, 2010, **39**, 3460–3471; (*b*) S. Dayal and C. Burda, *J. Am. Chem. Soc.*, 2007, **129**, 7977–7981; (*c*) M. Idowu, J. Y. Chen and T. Nyokong, *New J. Chem.*, 2008, **32**, 290–296.

9 W. R. Dichtel, J. M. Serin, C. Edder, J. M. J. Frēchet, M. Matuszewski, L. S. Tan, T. Y. Ohulchanskyy and P. N. Prasad, *J. Am. Chem. Soc.*, 2004, **126**, 5380–5381.

10 (*a*) J. Chen, K. Stefflova, M. J. Niedre, B. C. Wilson, B. Chance, J. D. Glickson and G. Zheng, *J. Am. Chem. Soc.*, 2004, **126**, 11450–11451; (*b*) C. C. Kang, C. T. Chen, C. C. Cho, Y. C. Lin, C. C. Chang and T. C. Chang, *ChemMedChem*, 2008, **3**, 725–728.

11 C. C. Chang, M. C. Hsieh, J. C. Lin and T. C. Chang, *Biomaterials*, 2012, **33**, 897–906.

12 (*a*) H. Ali and J. E. van Lier, *Chem. Rev.*, 1999, **99**, 2379–2450; (*b*) D. J. Ball, S. R. Wood, D. I. Vernon, J. Griffiths, T. M. A. R. Dubbelman and S. B. Brown, *J. Photochem. Photobiol., B*, 1998, **45**, 28–35; (*c*) V. Mantareva, V. Kussovski, I. Angelov, E. Borisova, L. Avramov, G. Schnurpfeil and D. Wöhrle, *Bioorg. Med. Chem.*, 2007, **15**, 4829–4835; (*d*) D. M. Guldi, T. D. Mody, N. N. Gerasimchuk, D. Magda and J. L. Sessler, *J. Am. Chem. Soc.*, 2000, **122**, 8289–8298.

13 (*a*) C. C. Chang, J. F. Chu, H. H. Kuo, C. C. Kang, S. H. Lin and T. C. Chang, *J. Lumin.*, 2006, **119**, 84–90; (*b*) B. K. An, S. K. Kwon, S. D. Jung and S. Y. Park, *J. Am. Chem. Soc.*, 2002, **124**, 14410–14415; (*c*) B. K. An, J. S. Lee, Y. S. Park, H. S. Song and S. Y. Park, *J. Am. Chem. Soc.*, 2004, **126**, 10232–10233.

14 (*a*) C. C. Chang, J. Y. Wu, C. W. Chien, W. S. Wu, H. Liu, C. C. Kang, L. J. Yu and T. C. Chang, *Anal. Chem.*, 2003, **75**, 6177–6183; (*b*) C. C. Chang, J. Y. Wu and T. C. Chang, *J. Chin. Chem. Soc.*, 2003, **50**, 185–188.

15 C. C. Chang, J. F. Chu, F. J. Kao, Y. C. Chiu, P. J. Lou, H. C. Chen and T. C. Chang, *Anal. Chem.*, 2006, **78**, 2810–2815.

16 A. P. Castano, T. N. Demidova and M. R. Hamblin, *Photodiagn. Photodyn. Ther.*, 2004, **1**, 279–293.

17 (*a*) A. C. Moor, *J. Photochem. Photobiol., B*, 2000, **57**, 1–13; (*b*) A. P. Castano, T. N. Demidova and M. R. Hamblin, *Photodiagn. Photodyn. Ther.*, 2005, **2**, 1–23; (*c*) N. Dias and C. Bailly, *Biochem. Pharmacol.*, 2005, **70**, 1–12; (*d*) M. E. Rodriguez, K. Azizuddin, P. Zhang, S. M. Chiu, M. Lam, M. E. Kenney, C. Burda and N. L. Oleinick, *Mitochondrion*, 2008, **8**, 237–246.

18 (*a*) N. L. Oleinick, R. L. Morris and I. Belichenko, *Photochem. Photobiol. Sci.*, 2002, **1**, 1–21; (*b*) J. Morgan and A. R. Oseroff, *Adv. Drug Delivery Rev.*, 2001, **49**, 71–86.

19 (*a*) C. A. Aliaga and J. C. Scaiano, *Org. Lett.*, 2003, **5**, 4145–4148; (*b*) M. E. Bulina, D. M. Chudakov, O. V. Britanova, Y. G. Yanushevich, D. B. Staroverov, T. V. Chepurnykh, E. M. Merzlyak, M. A. Shkrob, S. Lukyanov and K. A. Lukyanov, *Nat. Biotechnol.*, 2006, **24**, 95–99; (*c*) A. Roy, P. Carpentier, D. Bourgeois and M. Field, *Photochem. Photobiol. Sci.*, 2010, **9**, 1342–1350.

20 Y. S. Chou, C. C. Chang, T. C. Chang, T. L. Yang, P. J. Lou and T. H. Young, *J. Biomed. Biotechnol.*, 2012, DOI: 10.1155/2013/930281.